Mehran Ahmadi
Laboratory for Alternative Energy Conversion (LAEC),
Mechatronic Systems Engineering,
Simon Fraser University (SFU),
Surrey, BC V3T 0A3, Canada

Golnoosh Mostafavi
Laboratory for Alternative Energy Conversion (LAEC),
Mechatronic Systems Engineering,
Simon Fraser University (SFU),
Surrey, BC V3T 0A3, Canada

Majid Bahrami[1]
Laboratory for Alternative Energy Conversion (LAEC),
Mechatronic Systems Engineering,
Simon Fraser University (SFU),
Surrey, BC V3T 0A3, Canada
e-mail: mbahrami@sfu.ca

Natural Convection From Interrupted Vertical Walls

Steady-state external natural convection heat transfer from interrupted rectangular vertical walls is investigated. A systematic numerical, experimental, and analytical study is conducted on the effect of adding interruptions to a vertical plate. COMSOL multiphysics is used to develop a two-dimensional numerical model for investigation of fin interruption effects on natural convection. A custom-designed testbed is built and six interrupted wall samples are machined from aluminum. An effective length is introduced for calculating the natural convection heat transfer from interrupted vertical walls. Performing an asymptotic analysis and using a blending technique, a new compact relationship is proposed for the Nusselt number. Our results show that adding interruptions to a vertical wall can enhance heat transfer rate up to 16% and reduce the weight of the fins, which in turn, lead to lower manufacturing and material costs. [DOI: 10.1115/1.4028369]

Keywords: heat transfer, natural convection, interrupted wall, Nusselt number, asymptotic solution, experimental study, numerical simulation

1 Introduction

The design of efficient cooling system is essential for reliable performance of high power density electronics. Approximately 55% of failures in electronic devices are related to thermal effects [1]. In fact, the rate of such failures nearly doubles with every 10 °C increase above the operating temperature of power electronics [2]. With the ever-increasing power density and miniaturization in the electronics and telecom industry higher heat fluxes should be dissipated from the devices. Therefore, devising efficient cooling solutions to meet these challenges is of paramount importance and has direct impacts on the performance, service life and reliability of electronic, telecommunication, and power electronic devices.

Passive cooling is a widely preferred cooling method for electronic and power electronic devices since it is economical, quiet, and reliable. Natural air-cooling is also recognized as an important technique in the thermal design of electronic packages, because besides its availability and safety, it does not contaminate the air and does not add vibrations, noise and humidity to the system [3]. Such features of natural convection stimulated considerable research on the development of optimized finned heatsinks and enclosures [4–6]. Moreover, natural convection, and other passive cooling solutions (e.g., heat pipes), require no parasitic power which make them more attractive for sustainable and "green" systems. For instance implementing passive cooling techniques in telecom enclosures and shelters can reduce the parasitic energy required for thermal management from 25% of total input power to 15% in general [7] and zero percent in some cases [8].

The focus of this study is on natural convective heat transfer from interrupted, vertically mounted, rectangular walls as a fundamental element needed before analyzing fin arrays, heatsinks, and more complex geometries. As such, a general overview on pertinent literature in the area of natural heat transfer from fins is provided in this section. A variety of theoretical expressions, graphical correlations, and empirical equations have been developed to calculate the coefficients of natural convective heat transfer from vertical plates. Ostrach [9] made an important contribution on analyzing the natural convective heat transfer from vertical fins. He analytically solved laminar boundary layer equations using similarity methods for uniform fin temperature condition and developed a relationship for the Nusselt number for different values of Prandtl number. Merkin [10], also used similarity solution to solve natural convection heat transfer from a vertical plate with nonuniform wall temperature and wall heat flux. As well, Sparrow and Gregg [11] used similarity solutions for boundary layer equations for the cases of uniform surface heat flux. Churchill and Chu [12] also developed an expression for Nusselt number for all ranges of the Rayleigh, and Pr numbers. Yovanovich and Jafarpur [13] studied the effect of orientation on natural convection heat transfer from finite plates. Cai and Zhang [14] found an explicit analytical solution for laminar natural convection in both heating and cooling boundary condition. The focus of the available literature on natural convective from vertical plates has been on continuous rectangular walls.

Interruptions are discontinuities added in vertical walls to postpone the thermal boundary layer emergence in the channel flow between two adjacent walls; thus increase the total heat transfer rate [15]. Additionally, interruptions lead to considerable weight reduction, which in turn, can lower the manufacturing and material costs. A schematic for interrupted wall is shown in Fig. 1. It should be noted this arrangement is a more general form of geometry and includes both continuous and pin fins at the limit where the interruption length approaches zero and infinity, respectively. In other words, continuous and pin fins are two extreme cases of the targeted interrupted fins. Fin interruption is common in industry and has been extensively studied for internal natural convection [16,17] and forced convection [18]. However, to the authors' best knowledge no comprehensive study is available for natural convection from interrupted fins/walls. The present study aims to address this shortcoming.

The focus will be on the effects of fin length and interruption length. Also, to study the natural convective heat transfer from interrupted walls, a new concept "effective length," is introduced and a new compact relationship for the Nusselt number is developed based on nondimensional geometrical parameters.

2 Numerical Analysis

2.1 Governing Equation. We seek a solution for steady-state, laminar natural convective heat transfer from an isothermal vertically mounted interrupted wall, as shown schematically in Fig. 1. The conservation of mass, momentum, and energy in the

[1]Corresponding author.

Contributed by the Heat Transfer Division of ASME for publication in the JOURNAL OF HEAT TRANSFER. Manuscript received October 16, 2013; final manuscript received August 18, 2014; published online September 16, 2014. Assoc. Editor: Sujoy Kumar Saha.

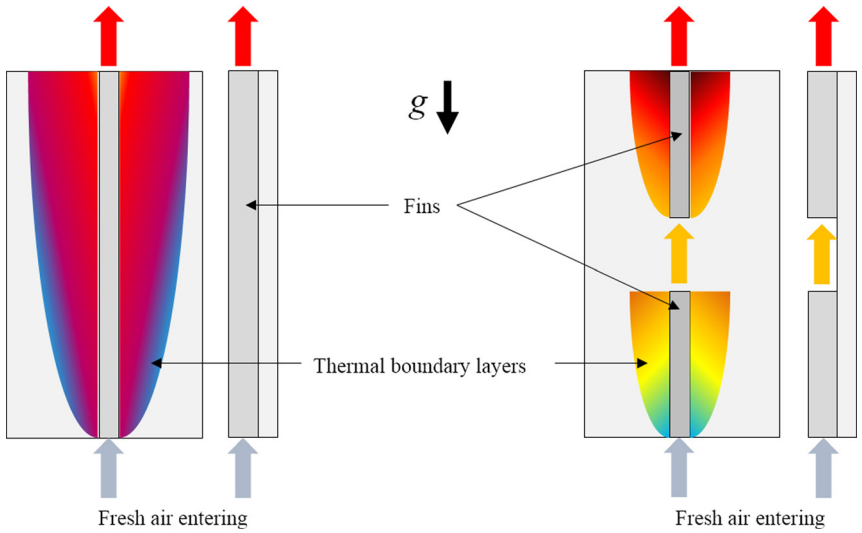

Fig. 1 Effect of interruptions on boundary layer growth in natural heat transfer from a vertical wall

domain are based on assuming a fluid with constant properties and the Boussinesq approximation [19] for density-temperature relation

$$\frac{\partial u}{\partial x}+\frac{\partial \upsilon}{\partial y}=0 \tag{1}$$

$$\rho\left(u\frac{\partial u}{\partial x}+\upsilon\frac{\partial u}{\partial y}\right)=-\frac{\partial P}{\partial x}+\mu\nabla^2 u \tag{2}$$

$$\rho\left(u\frac{\partial \upsilon}{\partial x}+\upsilon\frac{\partial \upsilon}{\partial y}\right)=-\frac{\partial P}{\partial y}+\mu\nabla^2\upsilon-\rho g \tag{3}$$

$$u\frac{\partial T}{\partial x}+\upsilon\frac{\partial T}{\partial y}=\alpha\nabla^2 T \tag{4}$$

where y is the direction parallel to the gravitational acceleration and x is the direction normal to the gravitational acceleration, u and υ are the velocity in x-direction and y-direction, respectively. Here, ρ, μ, and α are the fluid's density, dynamic viscosity, and thermal diffusivity, respectively.

Considering $(\partial P/\partial y)=(\partial P_\infty/\partial y)$, where P_∞ is the ambient hydrostatic pressure, and assuming Boussinesq approximation, Eq. (3) yields to

$$u\frac{\partial \upsilon}{\partial x}+\upsilon\frac{\partial \upsilon}{\partial y}=\nu\frac{\partial^2\upsilon}{\partial x^2}+g\beta(T-T_\infty) \tag{5}$$

where in our numerical simulations the buoyancy term, $-\rho_\infty g\beta(T-T_\infty)$, is added to the momentum equations as a body force term.

Inlet boundary condition is applied to the bottom of the domain which defines the boundary condition for the pressure at the inlet. As such, we assumed the gauge pressure to be zero. For the top and right side of the domain outlet boundary condition is applied, which imposes a constant pressure, the gauge pressure of zero in case of our problem. Symmetry boundary condition was chosen for the interruption region. This type of boundary condition is equivalent to a no-heat flux in the direction normal to the boundary plane. A no-slip isothermal solid surface is considered for the walls. Figure 2 shows a schematic of the domain considered for the numerical simulation, along with the chosen boundary conditions for the fins.

COMSOL multiphysics has been employed for solving the above-mentioned system of partial differential equations and mesh generation.

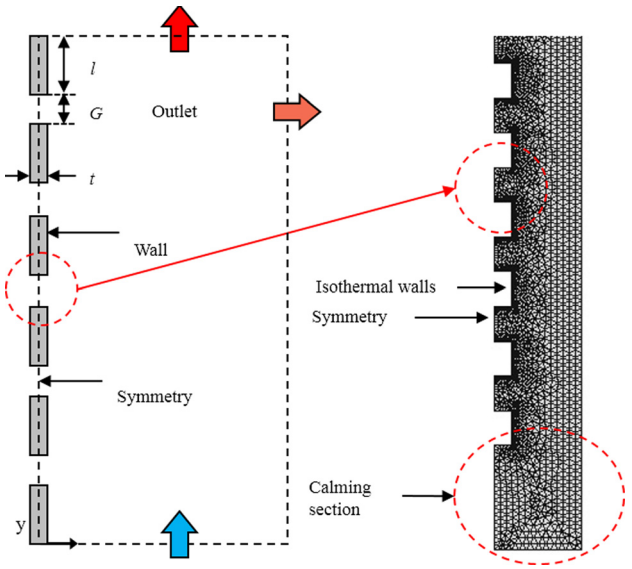

Fig. 2 (*a*) Schematic of the numerical domain and boundary conditions for vertical interrupted wall and (*b*) grid used in the model for interrupted wall

2.2 Mesh Independency. For simulating the heat transfer in the fins, a 2D model is created in COMSOL multiphysics 4.3, by coupling the fluid flow and heat transfer modules. As mentioned in Sec. 2, the coupling has been done by adding the Boussinesq buoyancy term, which is a function of temperature, to the momentum equation. A finer mesh size has been applied near the fin surface to resolve the boundary layer with an enhanced accuracy and an increasingly coarser mesh was chosen in the middle of the domain in order to reduce the computational time (see Fig. 2). Five different number of mesh elements are used for the benchmark cases and compared in terms of average heat flux from the walls to ensure a mesh independent solution. The parameters chosen for the benchmark case are shown in Table 1. Accordingly, for the mesh number of approximately 45,000, we found that the simulation gives approximately 0.01% deviation in average heat transfer rate from walls as compared to the simulation of fins with mesh number of 65,000, while for the number of elements less than 6500 the model does not converge to a reasonable solution. Figure 3 shows the mesh independence analysis for the

Table 1 Parameters used for the numerical simulation benchmark

Parameter	Description	Value	Unit
l	Fin length	5	(cm)
G	Gap length	2	(cm)
t	Fin thickness	1	(cm)
T_∞	Ambient temperature	20	(°C)
T_w	Wall temperature	60	(°C)
N	Number of fins	5	—

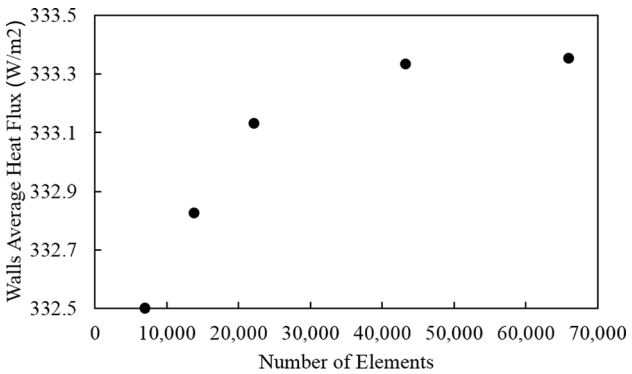

Fig. 3 Grid independency study; walls average heat flux versus number of elements for the benchmark case (see Table 1)

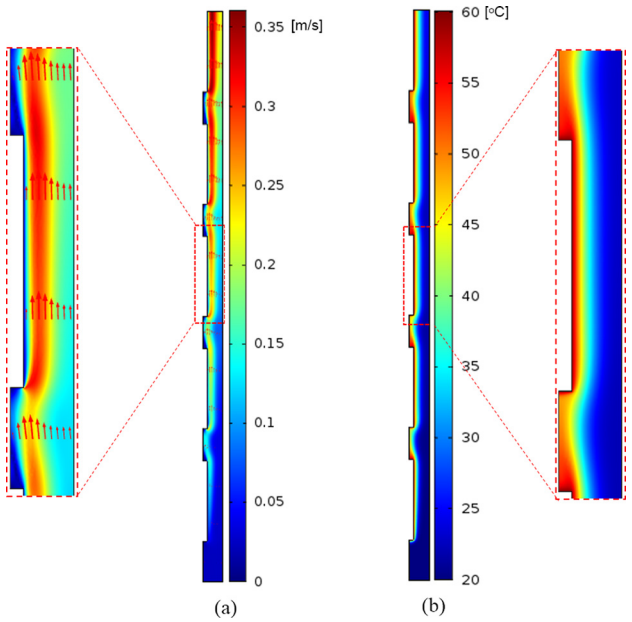

Fig. 4 (*a*) velocity domain and (*b*) temperature domain for the benchmarks case; the diffusion of velocity and temperature in the gap causes the air to reach the top wall with higher velocity and lower temperature

benchmark case. As the figure shows, the results are not too sensitive to the grid size.

The velocity and temperature domains are shown as results of the benchmark numerical studies in Fig. 4. As shown in the figure, the diffusion of velocity and temperature in the gap region, causes the air to reach the higher fin with higher velocity and lower temperature. This interruption in hydrodynamic and thermal boundary layers, is the main cause for the improvement of heat transfer from the fins.

3 Experimental Study

The objective of the experimental study is to investigate the effects of interruption length on the natural convective heat transfer from interrupted vertical walls, and also to validate the results from numerical simulations and mathematical modeling. To achieve this goal, a custom-made testbed is designed and built, and six interrupted wall samples with various geometrical parameters are machined from aluminum profiles. A series of tests with different surface temperatures are conducted. More details about the testbed design, test procedure, and uncertainty analysis is brought in the proceeding sections.

3.1 Testbed. The testbed is designed to measure natural convective heat transfer from interrupted vertical walls, as shown in Fig. 5(*a*). The setup included a metal framework from which the samples are hanged, and an enclosure made of compressed insulation foam with a thickness of 20 mm to insulate the back side of the samples. Inside the foam enclosure is filled with glass–wool to ensure the minimum heat loss from the backside of the baseplate. As such, any form of heat transfer from the back side of baseplate is neglected in our data analysis. The setup also includes a power supply, two electrical heaters, attached to the backside of the baseplate, T-type thermocouples, and three data acquisition (DAQ)[2] systems. Thermal paste (Omegatherm®201) is used to minimize the thermal contact resistance between the heater and the baseplate.

Six heatsink samples with the same baseplate width but different fin and interruption lengths are prepared. To fully investigate the effects of thermal boundary layer growth, different dimensions of the fins and interruptions are chosen, as listed in Table 2.

3.2 Test Procedure. The experiments are performed in a windowless room with an environment free of air currents. The room dimensions are selected to be large enough to ensure constant ambient temperature during the test. The input power supplied to the heaters is monitored and surface temperatures were measured at various locations at the back of the baseplate. Electrical power is applied using a variable voltage transformer (Variac SC-20M), and using DAQ systems (National Instruments, NI9225, and NI9227), the voltage and the current are measured to determine the power input to the heater. Eight self-adhesive, copper-constantan thermocouples (Omega, T-type) are installed in various vertical locations on one side of the baseplate, as shown in Fig. 5(*b*). Two extra thermocouples are installed on the same level with the highest and lowest thermocouples to make sure that the temperature is well distributed horizontally (T_9 and T_{10} in Fig. 5(*b*)). All thermocouples are taped down to the backside of the samples baseplate to prevent disturbing the buoyancy-driven air flow. One additional thermocouple is used to measure the ambient temperature during the experiments. Thermocouples are plugged into a DAQ system (National Instruments, NI9213). Temperature measurements are performed at ten points in order to monitor the temperature variation on the wall, and the average is taken as the baseplate temperature. Among all the experiments, the maximum standard deviation from the average temperature is 4 °C. Since the experiments are performed to mimic the uniform wall temperature boundary condition, the thickness of the baseplate and the fins are selected fairly high (10 mm) to ensure the minimum thermal bulk resistance and uniform temperature distribution in the samples. An infrared camera (FLIR, SC655) is used to observe the temperature difference between the baseplate and the fins. The maximum measured difference between the fins and the baseplate is about 2 °C, so for the data reduction, the fins are assumed to be at the same temperature with the baseplate. For each of the six samples, the experimental procedure is repeated for various power inputs. The baseplate temperature T_w, the ambient temperature T_∞, and the power input to the heater p_{input} are

[2]Data acquisition system.

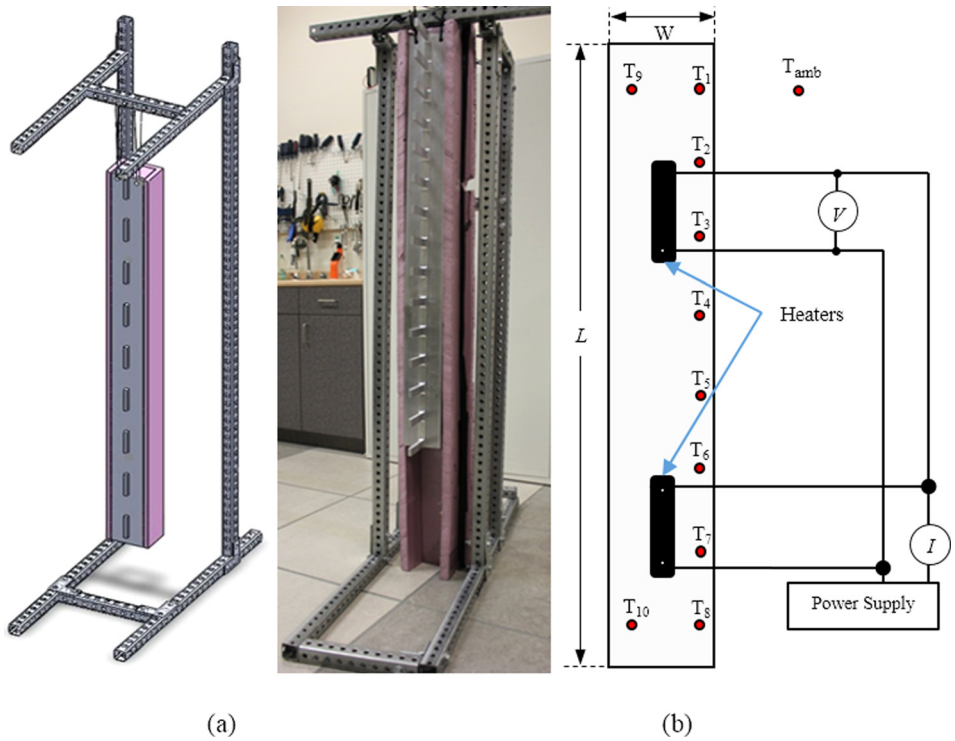

Fig. 5 (*a*) A schematic and photo of the testbed and (*b*) back side of the samples; positioning of the thermocouples and heater

Table 2 Dimensions of interrupted wall samples

Sample name #	l (mm)		n	G (mm)	L (m)	G/l	l/t
SW-1	50	14		50	1.35	1	5
SW-2	50	7		150	1.25	3	5
SW-3	50	10		100	1.40	2	5
SW-4	50	5		300	1.45	6	5
SW-5	50	10		150	1.85	3	5
SW-6	50	17		25	1.47	0.5	5

Note: Fin length base land width are constant in all the samples, $H = 100$ mm, $t = 10$ mm, and $W = 101$ mm.

Table 3 Range of the test parameters used in experimental studies

Parameter	Description	Range	Unit
m	Mass of the samples	1.2–2.1	(kg)
P	Heater power	30–150	(W)
T_∞	Ambient temperature	20–22	(°C)
T_w	Wall temperature	35–75	(°C)
Ra_l	Rayleigh number	10^5–10^8	—

recorded at steady-state considering the power factor equals to one. Table 3 lists the range of some important test parameters. The steady state condition is considered to be achieved when the rate of all temperature variations to be less than 0.1 °C/h, which in average, takes 150 min from the start of the experiment.

For the data reduction, the natural convection from the base-plate and fin tips are calculated using the available correlations in literature [12], and subtracted from total heat input to the system. Following Rao et al. [20], the effect of radiation heat transfer is also subtracted from the fins total heat transfer. Due to relatively low surface temperature and low emissivity of machined aluminum (between 0.09 and 0.1), the effect of radiation is not significant. The maximum calculated value for radiation heat transfer is 4.2% of total heat transfer.

3.3 Uncertainty Analysis. Voltage (V) and current (I) are the electrical parameters measured in our experiments, from which the input power, P_{input} can be calculated (see Eq. (7)). The overall accuracy in the measurements is evaluated based on the accuracy of the measuring instruments, mentioned in Sec. 3.2. The accuracy of the voltage and current readings are 0.3% for both parameters, based on suppliers' information. The reported accuracy values are given with respect to the instruments readings, and not the maximum range of measurement. The maximum uncertainty for the measurements can be obtained using the uncertainty analysis method provided in Ref. [21]. To calculate the uncertainty with the experimental measurements the following relation is used [21]:

$$\omega_R = \left[\sum \left(\frac{\partial R}{\partial x_i}\omega_i\right)^2\right]^{\frac{1}{2}} \tag{6}$$

where ω_R is the uncertainty in the general function of $R(x_1, x_2 \ldots x_n)$, and ω_i is the uncertainty of the independent variable x_i. The final form of the uncertainty for the input power becomes

$$P_{input} = VI \tag{7}$$

$$\frac{\delta P_{input}}{P_{input}} = \left[\left(\frac{\delta V}{V}\right)^2 + \left(\frac{\delta I}{I}\right)^2\right]^{\frac{1}{2}} \tag{8}$$

$$\frac{\delta \dot{Q}_{Rad.}}{\dot{Q}_{Rad.}} = \left[\left(4\frac{\delta T_w}{T_w}\right)^2 + \left(4\frac{\delta T_\infty}{T_\infty}\right)^2 + \left(\frac{\delta l}{l}\right)^2 + \left(\frac{\delta H}{H}\right)^2 + \left(\frac{\delta t}{t}\right)^2\right]^{\frac{1}{2}} \tag{9}$$

$$\dot{Q}_{N.C.}[W] = P_{input} - \dot{Q}_R \tag{10}$$

Plugging the values for $V, I, T_w, T_\infty, l, H,$ and t, into Eqs. (8) and (9), the maximum uncertainty value for $\dot{Q}_{N.C.}$ was calculated to be 8%. The measured temperatures uncertainty ΔT was $\pm 0.5\,^{\circ}C$. To calculate the heat transfer coefficient from measured $\dot{Q}_{N.C.}$ and ΔT, Eq. (11) can be used,

$$h = \frac{\dot{Q}_{N.C.}}{A\Delta T} \tag{11}$$

where

$$\frac{\delta h}{h} = \left[\left(\frac{\delta T_w}{T_w}\right)^2 + \left(\frac{\delta T_\infty}{T_\infty}\right)^2 + \left(\frac{\delta l}{l}\right)^2 + \left(\frac{\delta H}{H}\right)^2 + \left(\frac{\delta \dot{Q}_{N.C.}}{\dot{Q}_{N.C.}}\right)^2\right]^{\frac{1}{2}} \tag{12}$$

For the calculation of Nusselt number effective length, L_{eff} is used as the characteristic length, and since it is not measured, L_{eff} is not included in uncertainty analysis. Thermophysical properties such as thermal conductivity of air, are also assumed constant. Table 4 shows a list of parameters used in the uncertainty analysis with their calculated value. The amount of uncertainty for Nusselt number, which is calculated to be 10%, is shown as error bars on experimental data.

4 Results and Discussion

In this section, a new concept called "effective fin length" is introduced to calculate the Nusselt number for the natural convective heat transfer rate along the interrupted vertical fins. The effective length is obtained through equating the heat transfer rate from the actual interrupted wall with an imaginary continuous vertical wall, with the length of L_{eff}. The natural convection heat transfer from an isothermal vertical wall is well known subject and can be calculated from the following relationship [22]:

$$\mathrm{Nu}_{L_{eff}} = 0.59(\mathrm{Ra}_{L_{eff}})^{\frac{1}{4}} \tag{13}$$

knowing that

$$\mathrm{Nu}_{L_{eff}} = \frac{hL_{eff}}{k} \tag{14}$$

substituting $h = \dot{Q}/A\Delta T$ into Eq. (14) and using Eq. (13) one can find

$$L_{eff} = \left(\frac{\dot{Q}}{0.59k}\right)^2 \left(\frac{\alpha\nu}{g\beta}\right)^{\frac{1}{2}} \Delta T^{-\frac{5}{2}} \tag{15}$$

We also introduce ζ and γ, as follows:

$$\zeta = \frac{l}{t} \tag{16}$$

$$\gamma = \frac{G}{l} \tag{17}$$

Table 4 The uncertainty analysis parameters

Parameter	Maximum uncertainty
$\delta V/V$	0.3%
$\delta I/I$	0.3%
$\delta p/p$	0.4%
δT	$\pm 5\,^{\circ}C$
δH	0.1 (mm)
δl	0.1 (mm)
δt	0.1 (mm)
$\delta \dot{Q}_{Rad.}/\dot{Q}_{Rad.}$	7.5%
$\delta \dot{Q}_{N.C.}/\dot{Q}_{N.C.}$	8%

In order to develop a general model for all ranges of γ, two asymptotes are recognized and a blending technique [23] is implemented to develop a compact relationship for the effective length and the corresponding Nusselt number. The first asymptote is developed for small values of γ, where $\gamma \to 0$, for which the flow behavior resembles the flow over a vertical wall that has no interruptions with a total length of

$$L = Nl \tag{18}$$

where N is the number of fins. For the first asymptote, $\gamma \to 0$, the effective length is correlated using the present numerical results.

$$\frac{L_{eff,\gamma\to 0}}{N.l} = 0.22\gamma + 1 \tag{19}$$

The second asymptote is when $\gamma \to \infty$ that is the limiting case where the fins are located far enough from each other that they act as an individual fin. In other words, each fin's flow/heat transfer pattern will not get affected by the fins located at the bottom. For this asymptote, $\gamma \to \infty$, Eqs. (21)–(23), available in literature [4,9], are used to calculate the heat transfer from the wall. Natural convective heat transfer from the walls in this asymptote is the summation of heat transfer from all sides of the fin (bottom, two sides, and the top surface). The relationships used for calculating the heat transfer from the top, bottom, and sides of the wall are given in Ref. [24].

$$\dot{Q}_{total} = \dot{Q}_{ends} + \dot{Q}_{sides} \tag{20}$$

$$\mathrm{Nu}_{sides} = \mathrm{Nu}_l = 0.59\mathrm{Ra}_l^{\frac{1}{4}} \tag{21}$$

$$\mathrm{Nu}_{topside} = 0.56\mathrm{Ra}_l^{\frac{1}{4}} \tag{22}$$

$$\mathrm{Nu}_{bottomside} = 0.27\mathrm{Ra}_l^{\frac{1}{4}} \tag{23}$$

The natural convective heat transfer, $\dot{Q}_{N.C.}$, as calculated from the equations above, should be substituted in Eq. (15) to give the L_{eff} for larger values of γ, i.e., $L_{eff,\gamma\to\infty}$. As a result, for the top, bottom and sides of the wall, we can calculate the ratio of L_{eff}/Nl as

$$\frac{L_{eff,\gamma\to\infty}}{Nl} = N^{\frac{1}{3}}\left[0.83\left(\frac{1}{\zeta}\right)^{\frac{3}{4}} + 1\right]^{\frac{4}{3}} \tag{24}$$

Having $L_{eff,\gamma\to\infty}$ and $L_{eff,\gamma\to 0}$ available, a compact relationship for L_{eff} can be developed by using a blending technique, introduced by Churchill and Usagi [23],

$$L_{eff} = \left[\left(L_{eff,\gamma\to 0}\right)^c + \left(L_{eff,\gamma\to\infty}\right)^c\right]^{\frac{1}{c}} \tag{25}$$

where c is a fitting parameter, and its value is found by comparison with the present numerical data; the best fit is found for $c = -3$. This fitting parameter is found by minimizing the maximum percent difference between the model and the numerical data.

$\mathrm{Nu}_{L_{eff}}$ is calculated by substituting L_{eff} into Eq. (13). The final relationship is a function of, γ, ζ, N, and Ra, which in turn, is a function of temperature difference, as shown below:

$$\mathrm{Nu}_{L_{eff}} = \frac{hL_{eff}}{k} = 0.59\mathrm{Ra}_l^{\frac{1}{4}} N^{\frac{3}{4}} \left\{(0.22\gamma+1)^{-3} + \left[N\left(0.83\left(\frac{1}{\zeta}\right)^{\frac{3}{4}}+1\right)^4\right]^{-1}\right\}^{-\frac{1}{4}}, \quad \times 5 \le \zeta = \frac{l}{t} \le 15 \tag{26}$$

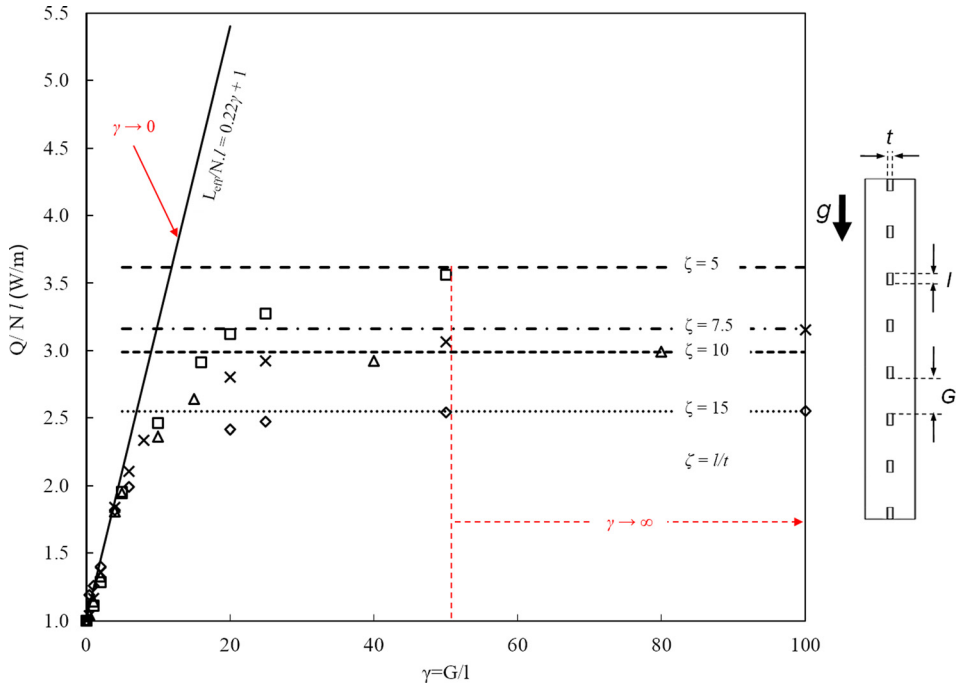

Fig. 6 Heat transfer versus $\gamma = G/l$ for different $\zeta = l/t$ values. The figure also shows the comparison between the numerical data (symbols) and introduced asymptotes (lines) for natural convection heat transfer from interrupted vertical walls.

where l is the fin length, ζ is the aspect ratio of the fin, $\zeta = l/t$, $\gamma = G/l$, N is the number of fins and Ra_l is the Rayleigh number based on fin length, respectively.

Figure 6 shows the asymptotic behavior of the natural convection from interrupted vertical walls for the two discussed limiting ranges of γ. Two different trends can be seen in the present data for the extreme values of γ. The first trend shows small values of γ and it can be seen that the data in this region is collapsed and matches a long vertical wall. The second trend corresponds to relatively large values of γ and shows a plateau, i.e., the asymptote for a single fin with the actual fin length ($L_{\mathrm{eff}} = l$).

Figure 7 shows the dimensionless proposed effective length, calculated using numerical data, as a function of γ. Asymptotic behavior of the effective length can be observed in the numerical data. We developed a new compact correlation for the effective length using a blending technique [23] as follows:

$$\frac{L_{\mathrm{eff}}}{N.l} = \left\{ [0.22\gamma + 1]^{-3} + \left[N^{\frac{1}{3}} \left(0.83 \left(\frac{1}{\zeta} \right)^{\frac{3}{4}} + 1 \right)^{\frac{3}{4}} \right]^{-3} \right\}^{-\frac{1}{3}} \tag{27}$$

The proposed correlation for the effective length is successfully compared against the numerical simulation results in Fig. 7. To calculate the Nusselt number from the numerical data, the average wall heat flux is obtained from the numerical simulations, and having the wall and ambient temperature, the heat transfer coefficient is calculated. Using the heat transfer coefficient, the calculated effective length, and thermal conductivity of the air the numerical Nusselt number is calculated. This enables developing a new compact relationship for Nusselt number based on the effective length, characterizing the natural convection heat transfer from interrupted vertical walls (Eq. (26)). This Nusselt number can be used to calculate the heat transfer rate for any rectangular interrupted fin in the range of $5 \leq \zeta = l/t \leq 15$. The parameter l/t represents the aspect ratio (slenderness) of the fins. For $l/t < 5$, the fin geometry will become closer to a cuboid (pin fin) and the correlations used to calculate the heat transfer are no longer valid. Also for $l/t > 15$, the fins will be too long and the effect of fin thickness will be negligible. This is while the effect of fin thickness is considered in our calculations and appears in Eqs. (26) and (27).

In Fig. 8 our experimental data obtained from the interrupted vertical wall samples (see Table 2) is compared against the proposed new relationship for the Nusselt number Eq. (26). Figure 8 also shows the numerical simulation results in very good agreement with experimental data. As it can be seen the proposed compact relationship is in very good agreement with both experimental and numerical results. The average relative difference between the relation and experiment is approximately 9% and the maximum relative difference is 15%.

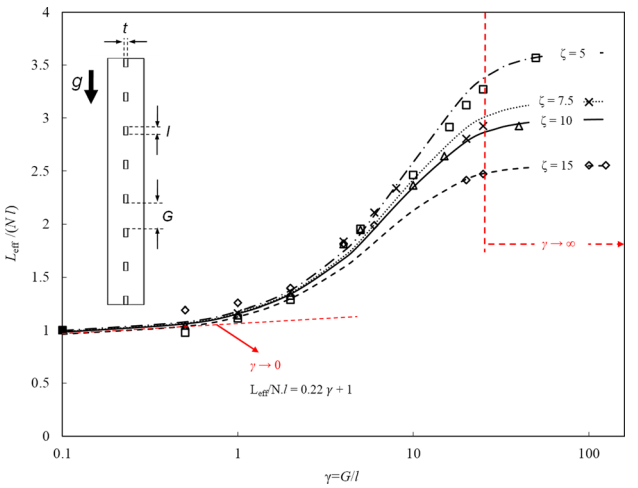

Fig. 7 Effective length versus $\gamma = G/l$ for different $\zeta = l/t$ values. The figure also shows the comparison between the numerical data (symbols) and the proposed relationship (lines) for the effective length (L_{eff}).

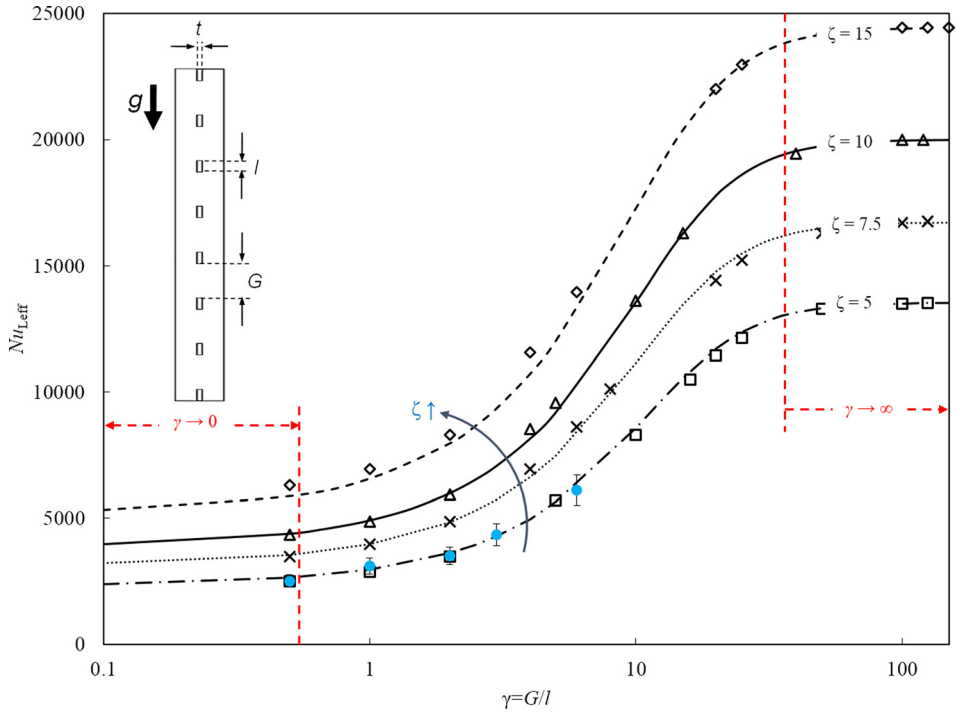

Fig. 8 Nusselt number versus $\gamma = G/l$ for different $\zeta = l/t$ values. The figure also shows the comparison between the numerical data (hollow symbols), experimental data (solid symbols), and the proposed compact relationship (lines).

5 Conclusion

Experimental, numerical, and analytical studies were performed to develop a compact correlation for natural convective heat transfer from vertical interrupted walls in this study. The effects of interruption length in natural convection were thoroughly investigated. The purpose of these interruptions was to reset the thermal boundary layer in order to decrease thermal resistance. A comprehensive numerical modeling was performed using COMSOL multiphysics. A custom-designed testbed was built and six aluminum interrupted wall samples were prepared and tested to verify the developed numerical and analytical models over the entire range of interrupted fin parameters. The collected data were successfully compared with the present numerical and analytical models. A new compact relationship was developed for the Nusselt number for natural convective heat transfer from interrupted fins using a blending technique, based on the nondimensional geometrical parameters $\gamma = G/l$ and $\zeta = l/t$. This relationship can be used for calculating heat transfer rate for any rectangular interrupted fin in the range of $5 \leq \zeta = l/t \leq 15$. The comparison of our experimental data to the available data in the literature [22], show that with the similar baseplate dimensions, interrupted fins can improve the heat dissipation up to 16% compared to a continuous vertical wall.

Nomenclature

A = surface area (m^2)
g = gravitational acceleration (m/s^2)
G = fin interruption length (m)
$Gr_{\mathcal{L}}$ = Grashof number ($Gr = g\beta\Delta T^3/\nu^2$)
h = convection heat transfer coefficient (W/m^2K)
I = electrical current (A)
k = thermal conductivity (W/mK)
l = fin length (m)
L = total length of fins (m)
L_{eff} = effective length (m)
m = mass of the sample (kg)
n = number of interruptions
N = number of fins in a column ($n = N - 1$)
Nu = Nusselt number (h/k)
P = pressure (Pa)
p_{input} = input power (W)
Pr = Prandtl number (ν/α)
$\dot{Q}$ = heat transfer rate (W)
Ra = Rayleigh number ($g\beta\Delta T^3/\alpha\nu$)
t = fin thickness (m)
T = temperature (K)
u = flow velocity in x-direction (m/s)
V = electrical voltage (V)
W = enclosure width (m)
x = direction normal to fin surface (m)
y = direction along fin surface (m)
v = flow velocity in y-direction (m/s)

Greek Symbols

α = thermal diffusivity (m^2/s)
β = coefficient of volume expansion ($1/K$) $\beta = U_{Sc}/U_D$
γ = interruption length to wall length ratio ($\gamma = G/l$)
ζ = wall length to wall thickness ratio ($\zeta = l/t$)
μ = dynamic viscosity ($kg/m \cdot s$)
ν = kinematic viscosity (m^2/α)
ρ = density (kg/m^3)

Subscripts

bottom = lower side of the fin/wall
NC = natural convection
R = radiation
side = vertical side of the fin/wall
top = upper side of the fin/wall
w = wall
∞ = ambient

References

[1] Zhang, M. T., Jovanovic, M. M., and Lee, F. C., 1997, "Design and Analysis of Thermal Management for High-Power-Density Converters in Sealed

Enclosures," Proc. APEC 97—Applied Power Electronics Conference, Vol. 1, pp. 405–412.
[2] Gurrum, S. P., Suman, S. K., Joshi, Y. K., and Fedorov, A. G., 2004, "Thermal Issues in Next-Generation Integrated Circuits," IEEE Transactions on Device and Materials Reliability, **4**(4), pp. 709–714.
[3] Chu, R. C., and Simons, R. E., 1993, "Recent Development of Computer Cooling Technology," International Symposium on Transport Phenomena in Thermal Engineering, pp. 17–25.
[4] Güvenç, A., and Yüncü, H., 2001, "An Experimental Investigation on Performance of Fins on a Horizontal Base in Free Convection Heat Transfer," J. Heat Mass Transfer, **37**(1), pp. 409–416.
[5] Yazicioğlu, B., and Yüncü, H., 2006, "Optimum Fin Spacing of Rectangular Fins on a Vertical Base in Free Convection Heat Transfer," J. Heat Mass Transfer, **44**(1), pp. 11–21.
[6] Bar-Cohen, A., 1984, "Optimum Thermal Spacing of Vertical, Natural Convection Cooled, Parallel Plates," ASME J. Heat Transfer, **106**(1), pp. 116–123.
[7] Lubritto, C., and Petraglia, A., 2008, "Telecommunication Power Systems: Energy Saving, Renewable Sources and Environmental Monitoring," IEEE Electrical Power and Energy Conference (EPEC), Vancouver, Canada, pp. 1–4.
[8] Hernon, D., Silvestre-Castillo, P., and Hayden, P., 2011, "Significantly Extending the Operational Range of Free Cooling in Radio Base Station Indoor Shelters," IEEE 33rd International Telecommunications Energy Conference (INTELEC), IEEE, Amsterdam, Netherlands, pp. 1–7.
[9] Ostrach, S., 1952, "An Analysis of Laminar Free-Convection Flow and Heat Transfer About a Flat Plate Parallel to the Direction of the Generating Body Force."
[10] Merkin, J., 1985, "A Note on the Similarity Solutions for Free Convection on a Vertical Plate," J. Eng. Math., **19**(1), pp. 189–201.
[11] Sparrow, E., and Gregg, J., 1956, "Laminar Free Convection From a Vertical Plate With Uniform Surface Heat Flux," Trans. ASME, **78**(1), pp. 435–440.
[12] Churchill, S. W., and Chu, H., 1975, "Correlating Equations for Laminar and Turbulent Free Convection From a Vertical Plate," Int. J. Heat Mass Transfer, **18**(11), pp. 1323–1329.
[13] Yovanovich, M., and Jafarpur, K., 1993, *Bounds on Laminar Natural Convection From Isothermal Disks and Finite Plates of Arbitrary Shape for All Orientations and Prandtl Numbers*, ASME-Publications-Htd, New York.
[14] Cai, R., and Zhang, N., 2003, "Explicit Analytical Solutions of 2-D Laminar Natural Convection," Int. J. Heat Mass Transfer, **46**(5), pp. 931–934.
[15] Fujii, M., 2007, "Enhancement of Natural Convection Heat Transfer From a Vertical Heated Plate Using Inclined Fins," Heat Transfer Asian Res., **36**(6), pp. 334–344.
[16] Daloglu, A., and Ayhan, T., 1999, "Natural Convection in a Periodically Finned Vertical Channel," Int. Commun. Heat Mass Transfer, **26**(8), pp. 1175–1182.
[17] Nada, S. A., 2007, "Natural Convection Heat Transfer in Horizontal and Vertical Closed Narrow Enclosures With Heated Rectangular Finned Base Plate," Int. J. Heat Mass Transfer, **50**(3–4), pp. 667–679.
[18] Ben-Nakhi, A., and Chamkha, A. J., 2007, "Conjugate Natural Convection in a Square Enclosure With Inclined Thin Fin of Arbitrary Length," Int. J. Therm. Sci., **46**(5), pp. 467–478.
[19] Bejan, A., 2004, *Convection Heat Transfer*, Wiley, New York.
[20] Rao, V. D., Naidu, S. V., Rao, B. G., and Sharma, K. V., 2006, "Heat Transfer From a Horizontal Fin Array by Natural Convection and Radiation—A Conjugate Analysis," Int. J. Heat Mass Transfer, **49**(19–20), pp. 3379–3391.
[21] Holman, J. P., 2001, *Experimental Methods for Engineers*, McGraw-Hill, New York.
[22] McAdams, W. H., 1954, *Heat Transmission*, McGraw-Hill, New York.
[23] Churchill, S. W., and Usagi, R., 1972, "A General Expression for the Correlation of Rates of Transfer and Other Phenomena," AIChE J., **18**(6), pp. 1121–1128.
[24] Goldstein, R. J., Sparrow, E. M., and Jones, D. C., 1973, "Natural Convection Mass Transfer Adjacent to Horizontal Plates," Int. J. Heat Mass Transfer, **16**(5), pp. 1025–1035.